PAPER

Check for updates

Investigating the effects of silk fibroin on ultrasound-mediated ultrafine bubble drug transport and delivery systems†

Nguyen Le Hanh Tran, Tam Vo Viet Tran, Khoi Le Minh Tran, Thu Phan Anh Le and Khoi Tan Nguyen [ID] *

Ultrafine bubbles with ultrasound stimuli have recently gained immense attention in developing drug delivery systems. However, research into their construction, stability and the factors influencing this aspect was conducted at the infant stage. This study aimed to utilize silk fibroin (a biocompatible protein extracted from *Bombyx mori* silkworm) in conjugation with polyethylene glycol 400 to stabilize the ultrafine bubble drug loading and releasing system. Light scattering laser imaging was used to examine the effects of SF and PEG on system stability. In addition, fluorescence laser imaging and optical absorbance measurements were performed to assess the role of these additives in the drug encapsulation and release process. Results confirmed the bubble stability was enhanced by the introduction of SF and PEG into the drug-carrier system. This study demonstrated that the proposed drug-transportation system possessed an encapsulation capacity of more than 80% and a substantial released drug content of up to 50% after the application of ultrasonic radiation.

Introduction

Drug delivery systems are methods or technologies designed to efficiently introduce drugs into the human body.[1] Conventional drug delivery systems using powder, capsules, tablets, *etc.*, however, have been criticized for their incapability to penetrate small blood vessels as well as the lack of release control.[2] These issues are primarily due to the intrinsic non-polar nature of most pharmaceutical compounds, resulting in their poor solubility in water, the main component of the bloodstream.[3] In addition, these drug-carrying vehicles are considerably large to pass through the narrow blood capillaries or overcome the immune system.[4] Consequently, these systems frequently suffer from low absorption and poor bioavailability.[5] Moreover, traditional delivery forms tend to release drugs in uncontrolled bursts with a high initial concentration that rapidly declines in the bloodstream, resulting in the inability to achieve the target release.[6] With recent advancements in nanotechnology, smart nanocarriers can overcome these challenges. These carriers are small in size and equipped with a stimuli-responsive mechanism, in which medicine molecules can be released to biological sites in response to either internal or external stimuli (*e.g.*, pH, optical, electrical, mechanical, and thermal)[2] External stimuli techniques have gained more attention since they can

be performed non-invasively and allow easier spatiotemporal manipulations of the releasing process.[7] Among these methods, ultrasound (US) has been widely used due to its non-invasive properties and its ability to simultaneously monitor images during the US application.[8,9]

Ultrasound refers to sound waves with a frequency greater than 20 kHz. All sound waves require a medium containing matters (in solid, liquid or gaseous phases) to propagate,[10] as particles within these media undergo a compression phase (high air pressure or density) and rarefaction phase (low air pressure or density) repetitively, creating a pressure wave.[11] Due to this nature, ultrasound can produce a series of thermal and mechanical bioeffects, in which the creation of cavitation is emphasized with the help of gas systems.[12] Cavitation occurs when vibration and oscillation are applied to air bubbles by an ultrasonic field. With low-density air filled inside the core, bubbles can expand and contract, corresponding to the compression and rarefaction phase changes of ultrasound.[12] The cavitation property of US and air bubbles was first harnessed in developing ultrasound contrast agents (UCAs) for diagnostics. Ultrasound contrast agents are small gas systems such as ultrafine bubbles (UFBs) and microbubbles (MBs).[13] Microbubbles typically range in size from 1 to 10 μm, whereas ultrafine bubbles are smaller than 1 μm.[14] MBs and UFBs were investigated to enhance the resolution of image generation *via* non-continuous (pulsed) ultrasound. The oscillation of the gas bubbles returns a secondary wave signal alongside the primary reflected ultrasound signal.[10] Stimuli-responsive drug release from ultrasound has also been developed from a similar

School of Biotechnology, International University, Vietnam National University of Ho Chi Minh City, 700000, Vietnam. E-mail: ntkhoi@hcmiu.edu.vn

† Electronic supplementary information (ESI) available. See DOI: https://doi.org/10.1039/d5ra00334b

cavitation mechanism. Microbubbles and ultrafine bubbles decorated with additives (*e.g.*, proteins, polymers, or monolayer lipids) can encapsulate hydrophobic drugs at their air/water interface.[15–17] When the gas core oscillates in response to the compression–rarefaction phase change, two types of cavitation can be produced: non-inertial and inertial.[18] Non-inertial cavitation exerts a repetitive oscillation on bubbles, thus gradually expanding the additive cover to release the pharmaceutical payload without rupturing the gas pockets (Fig. 1a).[12] On the other hand, inertial cavitation causes bubbles to increase in size beyond their elastic threshold and eventually collapse. The complete destruction can release all inner contents simultaneously, along with undesirable effects such as microjets or heat shocks (Fig. 1b).[12] These events can be controlled by selecting appropriate ultrasound waves. US beams with high-pressure amplitude and large mechanical index (an indication for the ability to cause cavitation effects) are known to produce inertial phenomena, whereas weaker ultrasound waves primarily cause non-inertial cavitation.[19]

For drug delivery systems, the gas systems used in conjunction with ultrasonic waves include both microbubbles and ultrafine bubbles. Between these, ultrafine bubbles have recently attracted more attention in therapeutic applications.[20–26] Compared with microbubbles, UFBs have a diameter of less than 1 μm, a more comparable size to effectively interact with biological cells. Consequently, these bubbles can travel in microvessels that are less than 20 μm[27] in diameter, thereby enhancing target drug delivery.[28] Additionally, the nanometer-scale dimensions of UFBs provide a larger surface area with more surface-active centers, thereby improving the drug-loading efficiency.[8]
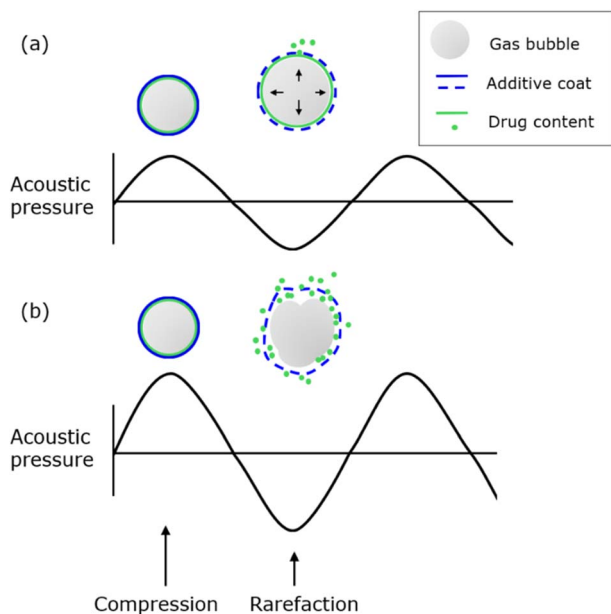

Fig. 1 Ultrasound-mediated drug release mechanism in gas bubble systems. (a) Non-inertial cavitation under low-pressure amplitude sound wave. (b) Inertial cavitation under high-pressure amplitude sound wave.

An emerging concern regarding the use of UFBs in drug transportation is their stability in bulk solutions. Calculations have indicated that for sizes ranging from 10 to 100 nm, gas diffusion in and out of air pockets occurs rapidly; thus, ultrafine bubbles can only exist in nanoseconds.[29] This transient existence raises questions about their reliability as a component in drug-delivery systems.[29,30]

One of the most common ways to enhance the lifetime of UFBs is to apply a monolayer surfactant coating on their gas/water interface to limit the mass transfer between the two phases. Surfactants, which can reduce the surface tension between two phases, are diverse in size and charge.[31] Compared with low molecular weight surfactants, proteins are considered better bubble stabilizers because of their thicker adsorbed layer, which lessens gas diffusion. This study investigated the effect of SF on stabilizing bubbles within drug delivery systems.[32,33] Silk fibroin (SF), a protein secreted from *Bombyx mori* silkworm, consists of heavy and light chains. The heavy chain contains 12 repetitive domains of GAGAGAGS (with G as glycine, S as serine, and A as alanine), forming a hydrophobic β-sheet crystallite.[34,35] On the other hand, its light chain is more hydrophilic due to its more non-repetitive charged and uncharged amino acid composition. Generally, proteins in bulk solution first dewet some hydrophobic side chains to adhere to the air–water interface. Its native structure can be subsequently unfolded, allowing the interior nonpolar core to be exposed to air while maintaining hydrophilic chains at the aqueous side of the interface.[36] Because of this sticking mechanism, silk fibroins reassemble into a rigid, branched structure to lower the surface tension and stabilize polar–nonpolar interfaces such as bubble surfaces, prolonging the bubble life.[37,38] Beyond the substantial stabilizing role, silk fibroin has been proven to be biocompatible, environmentally stable, biodegradable, and low-immunogenic, therefore, suitable for the introduction into a biological matrix.[39] In addition to surfactants, a low electrolyte concentration, typically the physiological salt level in blood, has been found to enhance UFB stability by forming an ionic shield to prevent bubbles from coalescence.[40] Therefore, in this study, a solution with sodium chloride at physiological concentration and SF was prepared to promote both stabilizing effects.[41,42] Another water-soluble and non-toxic additive, polyethylene glycol-400 (PEG-400), can also be introduced to preserve protein integrity and prevent its denaturation from any undesirable physical condition.[43,44] Along with being a protein stabilizer, PEG-400 can act as a cosurfactant. PEG-400 is expected to spread a stable film at the air–water or oil–water interface as its fairly hydrophobic –CH$_2$–O–CH$_2$– group can stick to the nonpolar air side. The aligned PEG chains on the interface can disturb the hydrogen network and reduce surface tension.[45] This property facilitates the emulsification of drugs to enhance the loading efficiency of oral, nasal, and intravenous delivery formulations.[46–50]

In our earlier research, we concentrated on albumin, a globular protein,[26] whereas this study focused on silk fibroin, a fibrous protein. The fibril-like characteristics of silk fibroin may lead to unique interactions at the air–water interface, potentially influencing drug release kinetics. The applied

loading and release mechanism is best suitable for hydrophobic drugs, such as flavonoids, which have an intrinsic high affinity to the bubble air/water interface facilitated by their aromatic rings. In this study, quercetin was used as the model drug.

As a flavonoid, quercetin comprises two phenyl rings (A and B) connected by a heterocyclic ring (C).[51] These hydrophobic rings enable quercetin to interact with hydrophobic sites on proteins, potentially inhibiting their activity. This mechanism contributes to its anti-cancer effects by suppressing leukocyte membrane proteins.[52] Additionally, quercetin's hydroxyl groups act as antioxidants, scavenging reactive oxygen species (ROS) and further supporting its anti-inflammatory properties.[53] The aforementioned surfactants and cosurfactants should be expected to enhance the stability of the matrix as well as provide certain effects on the quercetin loading and release capabilities.[54] This study contributes to the existing literature by providing additional data on silk fibroin's behavior at the air–water interface. It also explores the feasibility of using silk fibroin as an encapsulating agent in drug delivery systems, particularly bubble-based systems. Furthermore, this investigation examines the impact of incorporating PEG additives, offering insights into their role in enhancing system stability and efficiency.

Experimental

Materials

Bombyx mori silk fibroin 5% (w/v) was purchased from Sigma Aldrich. The other chemicals used in this study were ethanol (99.7%, Xilong Scientific), quercetin (Sigma Aldrich), and polyethylene glycol-400 (Sigma Aldrich). Sodium chloride (99.5%, Sigma Aldrich) was heated to 300 °C for 8 hours to remove impurities. A Milli-Q ultrapure water system (Millipore, USA) with a resistivity of 18.2 MΩ cm was used to prepare the solutions in this research.

Table-top ultrasonic bath (Derui, DR-MS13, 20 kHz), UV-Vis spectrophotometer (JASCO, model V-730), high-frequency acoustic wave generator (Portable Ultrasound, 1 MHz), centrifuge (HERMLE LaborTechnik, model Z306), monochromatic 10 mW 532 nm continuous wave laser (PGL-XII-E-532, CNI laser), continuous wave diode laser source of the 405 nm violet beam, and CCD camera (Matsushita, 7.5 MP, Venus Engine III) were the instruments employed in the experiments.

Methods

Preparation of samples/controls and procedure of loading quercetin. Samples were first prepared using sodium chloride and quercetin in ultrapure water. The salt concentration in the final solution was 154 mM to mimic the human physiological condition and to produce a bubble-stabilizing effect. Quercetin was maintained at 50 μM, consistent with a previous study in which the same drug was loaded using UFBs.[26] The solutions were sonicated in the 20 kHz bath for 40 minutes in two constituent stages. The first 20 minutes were with the two aforementioned components (*i.e.*, NaCl salt and quercetin) for UFB generation and quercetin adsorption. This sequence

ensured that quercetin was loaded onto the bubbles before the surfactants, preventing premature adsorption of surfactants to the air/water interface, which could hinder drug loading. Due to the nonpolar nature of flavonoids, quercetin can be attracted to the gas core of UFBs. The hydrophobic forces between quercetin and gas molecules can position the drug for a short period, enabling surfactant encapsulation.[55] Consequently, the adsorption coated a quercetin shell on the air/water interface of the generated bubbles. This also helped prevent gas diffusion into the environment, allowing the bubbles to last temporarily.[26]

In the subsequent 20 minutes, SF and PEG-400 were carefully transferred into the container to develop a protective film outside the quercetin-UFB system. The loading procedure is illustrated in Fig. 2a. Throughout the procedure, the sonication bath was coupled with a cooling system to strictly control the experimental conditions.

The silk fibroin concentration was first chosen at 10 μg mL^{-1} (or 0.10 μM), whereas PEG-400 at 2% compared with the introduced SF volume (v/v$_{SF}$) (or 564 μM) was chosen due to their good performance during preliminary research. This sample was named S10P2. In this study, investigations on these two additives were conducted using formulations of lower amounts since the smaller the amounts of these proteins and polymers, the less impact the drug delivery system imposes on the biological matrix. For instance, silk fibroin concentration could be reduced to 5 μg mL^{-1} (0.05 μM) and PEG-400 to 1%(v/v$_{SF}$) (282 μM), giving another three tested samples, namely, S10P1 – with 0.10 μM of SF and 282 μM PEG, S5P2 – with 0.05 μM of SF and 564 μM of PEG, and S5P1 – with 0.05 μM of SF and 282 μM of PEG.

In addition to the different formulations of SF and PEG-400, three control formulations were prepared for the experiments, as illustrated in Fig. 2b. Each would lack one or both of those additives, listed as control without both silk fibroin and polyethylene – C-Ø, control containing only SF – C-SF, and control containing only PEG – C-PEG, to demonstrate the imperative role of the protein and polymer in the proposed drug transportation and delivery system. Table S1† summarizes the details of the samples and controls used in this study.

Investigation of the stability of the loading system. The stability of the UFB system is described by the change in the bubble number density over a period of observation. The bubble number density in each loaded sample was represented by the elastic scattering intensity. The experimental setup and methodology followed that of a previous study.[56] As illustrated in Fig. 3, a 532 nm CW laser was used to direct the light through the sample/control, and the scattered solution was captured by the camera. Subsequently, the images were analyzed using ImageJ software (Version 1.53, the National Institutes of Health) with a Color Histogram function to decompose the color into three channels, red-blue-green. The software then reported the average values for each channel from 0 to 255 (for 8-bit image). The higher the value, the closer the color came to white, indicating that it was more scattered. Given that only green 532 nm photons were emitted by the laser and the bubbles, the green
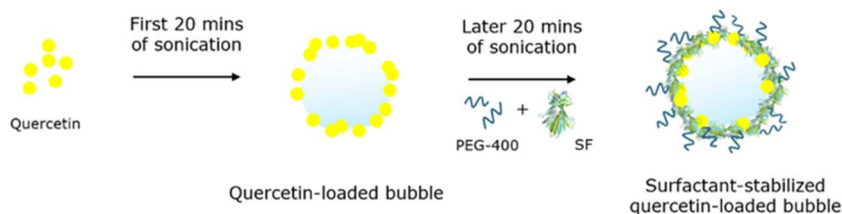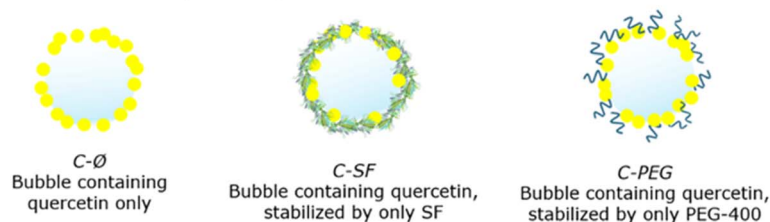
Fig. 2 Illustration of (a) quercetin loading and surfactant introduction procedure with two consecutive sonication periods and (b) different controls for removal of one or both additives in the later sonication period.

channel value of each image was extracted as the scattering intensity.

The solutions were observed over 1 hour, starting after the completion of 20 kHz sonication, with images captured every 10 minutes. This timeframe was chosen considering that the infusion time for the UFB system into a host system persists for 15–30 minutes and the transit time of bubble systems through the bloodstream to reach target sites ranges from seconds to minutes. The initial points (at 0th min) served as a reference to normalize the later data from the green channel value into relative scattering intensity (%). Subsequently, the relative scattering intensities were used to calculate $\Delta_{scattering}$ of the solutions using the following formula:

$$\Delta_{scattering} = I_{(scattering\ at\ 0th\ min)} - I_{(scattering\ at\ 60th\ min)} \qquad (1)$$

where $I_{scattering}$ is the relative scattering intensity (%) computed from the green channel values. The $\Delta_{scattering}$ represented how much of the bubble content had disappeared compared with the initial observation, which is inverse to the bubble stability. All four samples and three controls were tested. For each sample/control, there would be five $\Delta_{scattering}$ values from five independent replicates, and they were used for six one-tailed Mann–Whitney U tests between the chosen system S10P2 with three controls and three other formulations. By comparing the p-value of each pair to alpha = 0.05, this could evaluate the effects of different surfactant concentrations on the system stability and highlight the contribution of PEG and SF. Mean values and positive–negative standard deviations were depicted on line graphs plotting each sample/control $\Delta_{scattering}$ over time.

Confirmation of the loading success of the bubble system. The success of the drug loading procedure was determined by analyzing the drug interactions with solvent and surfactant molecules.[26]

Two similar S10P2 samples were prepared but underwent different treatments: one with the same 20 kHz sonication
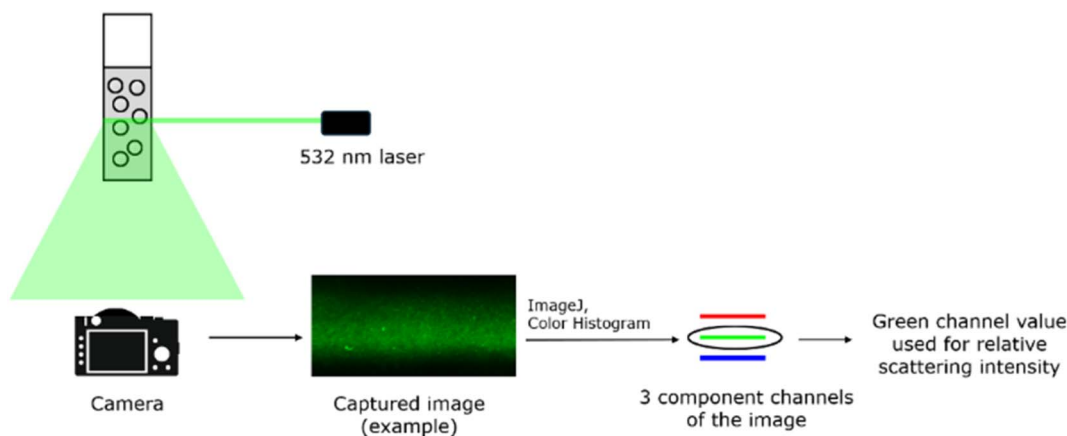

Fig. 3 Diagram of the green laser scattering experiment for loaded samples/controls.

procedure as the bubble system preparation step described and one without any sonication. The two samples were subsequently analyzed using a UV-Vis spectrophotometer over a wavelength range of 300–500 nm. The measured spectra were evaluated to provide several insights into the loading success.

Calculation of the loading efficiency. Drug loading efficiency (LE%) was defined as the percentage of quercetin successfully loaded on bubbles compared to the introduced amount (50 μM). The loaded samples/controls were centrifuged at 6000 rpm for 40 minutes to disrupt the bubble systems and settle the loaded quercetin into the pellet.[57] The supernatant, representing the unloaded quercetin amount, was scanned for absorption at 300–500 nm using a UV-Vis spectrophotometer. Unloaded molecules are quercetin fully solvated in the bulk solution, and they are characterized by a 368 nm peak from UV-Vis spectra.[58,59] A series of solutions with different fully solvated quercetin concentrations were prepared and measured with a UV-Vis spectrophotometer for the same wavelength range. The peak area was plotted against the known fully solvated quercetin concentration to develop a standard curve. Afterward, the peak area of the supernatants in the samples/controls was used to calculate the unloaded quercetin concentration, and the loading efficiency was calculated as follows:[26]

$$\text{LE\%} = \frac{[\text{QCT}]_{\text{initial}} - [\text{QCT}]_{\text{supernatant}}}{[\text{QCT}]_{\text{initial}}} \times 100\% \qquad (2)$$

where $[\text{QCT}]_{\text{initial}}$ is the total or initially introduced quercetin concentration (equal to 50 μM), and $[\text{QCT}]_{\text{supernatant}}$ is the quercetin concentration obtained from the supernatant peak area or the unloaded one. The expression '$[\text{QCT}]_{\text{initial}} - [\text{QCT}]_{\text{supernatant}}$' represented the loaded drug concentration. This experiment was performed using the most effective SF-PEG formulae from the stability test (in this case, S10P2 and S5P2) and the three controls. Each task was performed in triplicate independently. In addition, these LE% results are represented as column charts with mean values and standard deviation error bars for further comparison. Mann–Whitney U test was performed for each sample *versus* each control. *P*-Value was compared with $\alpha = 0.05$ to compare the average efficiencies.

Procedure of releasing quercetin. After drug loading by sonication at 20 kHz, quercetin underwent another sonication for drug release using a 1 MHz ultrasound transducer. One megahertz is the frequency commonly used for clinical applications to produce the non-inertial cavitation effect, thereby preventing harmful results from biological bodies.[55,60] The container of the loaded solution was covered with a thin film of ultrasound coupling gel. The 1 MHz probe was then applied to the gel for 5 minutes at an output intensity of 1.6 W cm^{-2} and 8% duty cycle for quercetin release.[26]

Confirmation of the releasing success. The hydrophobic interaction of quercetin with nonpolar molecules such as ambient air in UFBs exhibits a distinctive red fluorescence upon excitation at 405 nm.[61] As quercetin is released out of the UFB system and into the aqueous solution, this interaction no longer exists; thus, no fluorescence is produced or detected.[62] This on–off mechanism provides an approach to confirm the success of

the release procedure. However, when quercetin is released into the bulk solution, it may aggregate under hydrophobic driving force.[63] This aggregation can produce additional red fluorescence, potentially obscuring the light emission of loaded quercetin and introducing noise into the experiment. To address this issue, after release, samples were first subjected to aggregation removal. The samples were centrifuged at 1500 rpm for 5 minutes to settle the aggregates as pellets. The supernatant was then removed using a syringe with a 0.5-mm needle.[64] Subsequently, the solutions were placed in front of a 405 nm laser for quercetin excitation. The images were also captured by the camera and analyzed by ImageJ's Color Histogram for a three-channel subdivision. The red channel values were collected to represent the fluorescence intensity. The images were taken before and after the application of 1 MHz sonication to detect changes in fluorescence.

The S10P2 sample was prepared five times independently, and its 'before released' and 'after released' red channel values were used to perform the Wilcoxon signed-rank test. The p-value was compared with $\alpha = 0.1$ to confirm the success.

Calculation of releasing efficiency. Releasing efficiency (RE%) was calculated as the percentage of released quercetin amount relative to the loaded concentration, which was calculated from the expression '$[\text{QCT}]_{\text{initial}} - [\text{QCT}]_{\text{supernatant}}$' in eqn (2). In contrast, Fig. 4 describes the computation of the released amount, by taking the difference between the loaded amount and quercetin concentration remaining on the bubbles after release (denoted as 'remained'). Since quercetin content can be quantified from its fluorescence intensity,[62,65] a standard curve was constructed to provide the correlation between the remaining quercetin amounts and the red channel values (Fig. 4). From this curve, the red channel values of each sample/control were used to calculate the remaining quercetin concentration.

Releasing efficiency RE% was then computed using the following formula:

$$\text{RE\%} = \frac{[\text{QCT}]_{\text{released}}}{[\text{QCT}]_{\text{loaded}}} \times 100\% \qquad (3)$$

where $[\text{QCT}]_{\text{loaded}}$ is the loaded concentration calculated from '$[\text{QCT}]_{\text{initial}} - [\text{QCT}]_{\text{supernatant}}$' and $[\text{QCT}]_{\text{released}}$ is the released amount computed from the procedure in Fig. 4. Statistically, the same samples/controls used for the LE% test were used in this experiment. The RE% results are also displayed in column charts with the corresponding positive and negative error bars. Then, the Mann–Whitney U test ($\alpha = 0.05$) was performed with each sample–control pair to compare the efficiency.

Results and discussions

The development of a drug-delivery system encompasses two critical aspects: drug transport and drug delivery. Drug transport accounts for the distribution of molecules in the bloodstream to the target site; therefore, this process depends on the stability of the system. Conversely, drug delivery can be broken down into drug loading and drug release processes. The experimental results from this study indicate that the
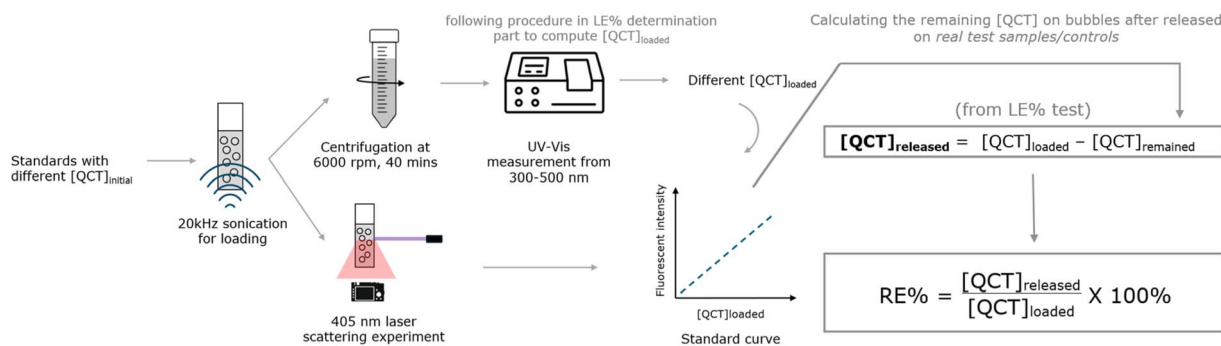
Fig. 4 Diagram of developing the standard curve between loaded quercetin concentrations and their red value as well as illustrating how to use the curve in calculating the released quercetin amount in released samples/controls.

surfactants, silk fibroin and PEG-400, might influence these two phases.

Stability of loading systems

Comparison S10P2 with controls. Fig. 5 illustrates the relative scattering intensity at seven time points, from the initial observation point (0th min) to the final measured point (60th min). Each replication of the loaded samples/controls would report a $\Delta_{\text{scattering}}$ value after 1 hour.

The statistical results from the one-tailed Mann–Whitney U test comparing the S10P2 system with the three controls (Table S2†) showed that the formulation with both surfactants showed a significantly lower $\Delta_{\text{scattering}}$. The comparison elucidated that the combined presence of SF and PEG improved the stability of the drug-loading UFB system over time compared with the presence of no surfactant or only one surfactant.

Comparison among different SF-PEG formulations. Similarly, the 0th and 60th min data points in Fig. 6 were used to calculate the $\Delta_{\text{scattering}}$ values for each replication of the four samples. According to the statistical results from the one-tailed Mann–Whitney U test comparing four different SF-PEG formulations (Table S3†), S10P2 displayed a significantly lower $\Delta_{\text{scattering}}$ value, indicating higher stability over time.

Specifically, S10P2 was significantly more stable than S10P1 and S5P1, but comparable to S5P2. It also showed that S10P2 had smaller error bars, demonstrating better consistency in the loading system. These results indicated that different ratios of SF and PEG present different influences on system performance.

The most stable formulations were those with both surfactants, and the large amount of PEG-400 contributed greatly to the system, as can be seen in S10P2 (Fig. 5) and S5P2 (Fig. 6).

An explanation for this was that SF might work as the primary surfactant to create a rigid shell outside the bubbles, thereby extending their lifetime. However, due to its small size ($MW_{\text{PEG-400}} = 0.3$ kDa), the addition of PEG-400 allows it to fill in the intermolecular gaps between large silk fibroin structures (average $MW_{\text{SF}} = 100$ kDa), thus preventing further gas diffusion, which reduces bubble collapse.[66] In addition, it is worth noting that in C-Ø, although there were no surfactants, the scattering intensity appeared to be as high as the other controls. As mentioned, quercetin can adsorb on the air/water interface of bubbles and help prevent mass transfer. This phenomenon may help to preserve a high concentration of freshly produced UFBs, nevertheless, the effects are only temporary, resulting in poor stability over time.

Although the scattering laser imaging results showed a noticeable difference in intensity reduction between test samples and controls, there was uncertainty due to the lack of investigation into the size of the bubbles inside the solution, which may have contributed to the scattering phenomenon.[67] Here in this study, it is hypothesized that adsorbed SF, PEG-400 and NaCl layers can effectively prevent cross-bubble interactions.

Fig. 5 532 nm laser light scattering intensity monitored in an hour from four samples: the chosen formulae S10P2 and three controls C-Ø, C-SF, and C-PEG. The error bars represent the standard error of the mean (SEM) of five repetitions for each sample at each observation time point.

Loading effects of the bubble system

Confirmation of the loading success. In this experiment, the two samples were similar in terms of content, with the same amount of NaCl, QCT, SF, and PEG; the only difference was the presence or absence of UFBs. Fig. 7 illustrated that without
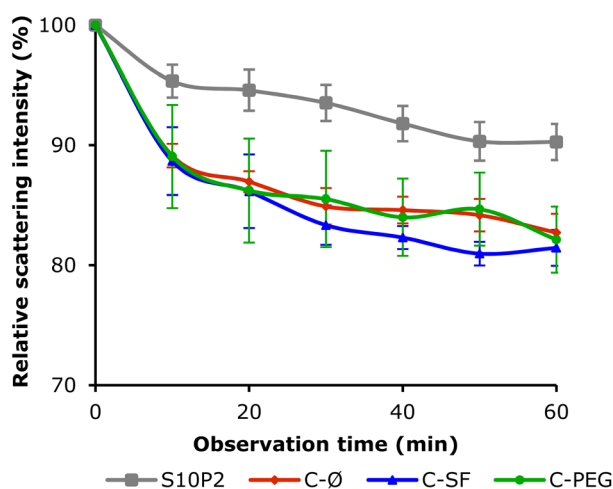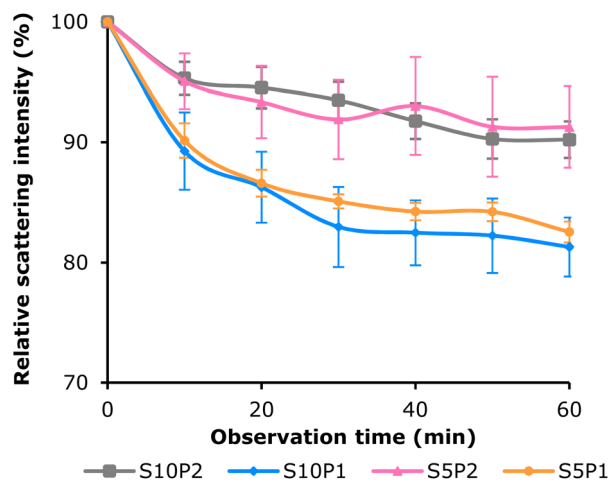
Fig. 6 UV-Vis spectra change from without bubbles (black curve with one fitted peak at 368 nm) to with bubbles (four red curves with fitted peaks at 324, 368, 374, and 423 nm from left to right) in quercetin-containing samples with both SF–PEG.

Fig. 8 Quercetin structure with the named rings, A, B, and C.[69]

bubbles, the UV-Vis spectrum revealed only one peak at 368 nm. Introducing bubbles reduced this peak and revealed the emergence of three more peaks at 324, 374, and 423 nm. Before being transferred into to the sample solution, quercetin was prepared in ethanol. While fully solvated by ethanol molecules, quercetin exhibits an absorption band of 300–400 nm, by the interaction of rings B, C (in Fig. 8) and solvent molecules.

Their resulting cinnamoyl system is commonly observed with a maximum peak at 368 nm.[58,59] This phenomenon was demonstrated clearly in the sample without bubbles, confirming that quercetin might still be in the fully solvated form, without any interactions with air bubbles or surfactants.

When bubbles were introduced into the system, the 368 nm peak declined. As mentioned, flavonoids like quercetin possess the ability to adsorb onto the air/water interfaces due to their hydrophobic interactions with the gas core.[68] Since silk fibroin has both negative and positive sites as well as a hydrophobic core, it is likely to have SF perform the aforementioned interactions with quercetin, resulting in emerging peaks.
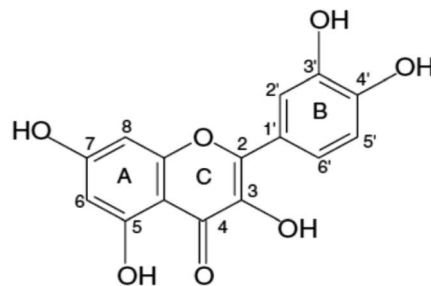
The decrease in absorbance at 368 nm might have resulted from the movement of quercetin from being fully solvated in bulk solution to partially bound on the bubble surface, indicating the successful loading of the drug to the system. In addition, the other three shifted peaks besides the 368 nm peak in Fig. 7 illustrate that quercetin interacts with the surfactant layer adsorbed on the air/liquid interface of the bubbles. Amphiphilic structures such as surfactants were found to shift quercetin's maximum absorption to longer wavelengths by both hydrophobic and electrostatic forces.[59] In this case, anionic surfactants were more likely to interact with quercetin by hydrophobic force at ring B, thus changing the corresponding absorption band 300–400 nm and creating new peaks at 374 and 423 nm. Conversely, cationic surfactants can deprotonate quercetin at 3 and 7 positions (Fig. 8), altering another absorption band from rings A and C, 240–280 nm, and causing a new peak at 324 nm.

Determination of loading efficiency. The standard curve used to calculate the solvated quercetin concentration was also based on the maximum absorption at 368 nm when the quercetin molecules were surrounded by solvent molecules. The established curve is shown in Fig. S1.† The LE% values calculated from eqn (2) are illustrated in the following chart. A comparison between two samples (S10P2 and S5P2) and three controls (C-Ø, C-SF, and C-PEG) was conducted using one-tailed Mann–Whitney U tests. The results are shown in Table S5.† According to the tests, the samples only had a better or equal loading efficiency than C-PEG, while being outperformed by the
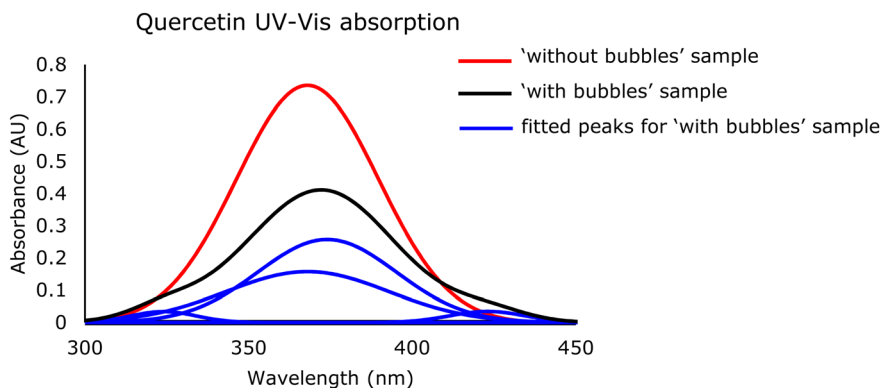

Fig. 7 532 nm laser light scattering intensity monitored in an hour from four samples: selected S10P2 and three other formulations, S5P2, S10P1, and S5P1. The error bars represent the standard error of the mean (SEM) of five repetitions for each sample at each observation time point.

other two controls. When comparing the two samples, S10P2 also displayed a slightly poorer LE% compared to S5P2, which was absent of 5 µg mL^{-1} (0.05 µM) in SF concentration. However, both samples exhibited a loading efficiency of greater than 80%, which was equivalent to more than 40 µM of quercetin delivered at once.

It appeared that the high concentrations of surfactants in S10P2 and S5P2 seemed to replace a small amount of quercetin at the interface during the 20 kHz sonication, which led to their slightly lower LE% compared to C-Ø and C-SF (Fig. 9). Regarding C-PEG, the SD error bars showed the inconsistency of loading capability when introducing PEG alone to the bubble system. Compared with the apparent hydrophobic regions on SF, PEG-400 contains only an uncharged but polar chain, which means it has less affinity to the air/water interface of the bubbles.[70] Together with the poorer adsorption to the interface, polyethylene glycol 400 does not display significant interactions with quercetin like SF; thus, the loading efficiency in the replicates was more arbitrary as a result from the unstable coating.

Overall, it can be inferred that the lower the surfactant concentration in the system, the higher the drug loading efficiency due to less adsorption competition against the bubble decorating layer. According to the chart, the sample without any additives (C-Ø) showed the highest LE%. Whereas the sample with only SF dropped the efficiency slightly, the addition of only PEG significantly affected the LE%.

Releasing effects of the bubble system

Confirmation of releasing success. The red channel values of five S10P2 samples before and after the 1 MHz release process were grouped to perform the Wilcoxon signed-rank test
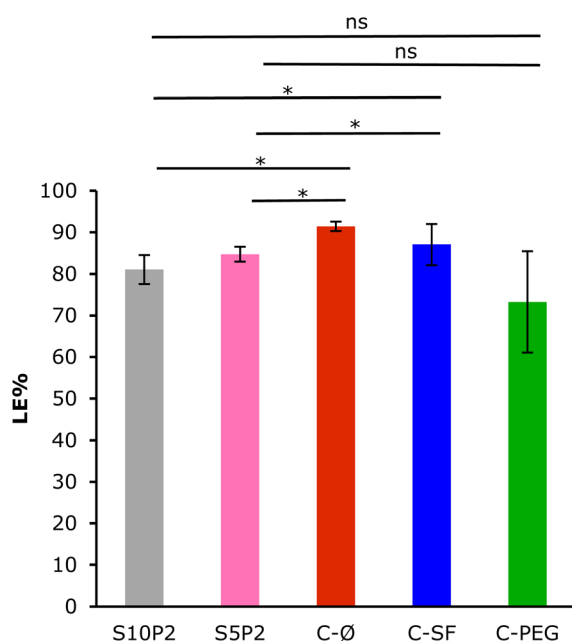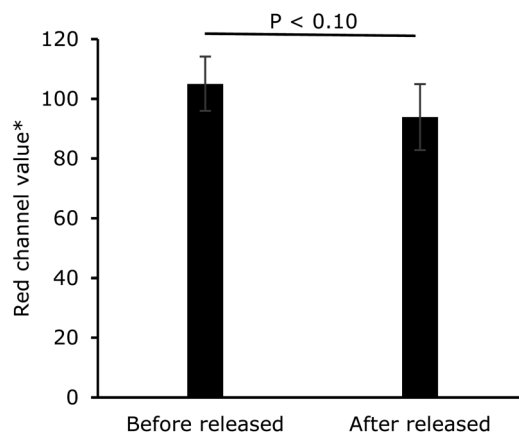
Fig. 10 Red channel values of sample 'before the releasing process' and 'after the releasing process'. *Red channel value was the average red color intensity of all pixels in images, ranging from 0–255 (8 bit), detected by ImageJ.

(Fig. 10). The release process by 1 MHz sonication created a substantial drop in the fluorescence of the drug. This decrease indicated the successful liberation of the drug from the bubble system, as quercetin stopped producing light emission.

Determination of releasing efficiency. The standard curve described in Fig. 4 was reported in Fig. S2.† The measured red channel values of two samples, S10P2 and S5P2, as well as those of three controls, are summarized in Table S6,† together with their corresponding remained and released concentrations. The releasing efficiency is reported in the following chart and used to perform one-tailed Mann–Whitney U tests comparing the mean differences. One-tailed Mann Whitney U tests were performed to compare two samples, S10P2 and S5P2, with three controls, C-Ø, C-SF, and C-PEG. From the results in Table S7,† the releasing efficiency seemed to be more similar between the samples and controls than LE%. Both S10P2 and S5P2 produced similar loading (Fig. 9) and releasing amounts (Fig. 11) of quercetin from the system despite the difference in the silk fibroin concentration. However, the S10P2 formulation showed better consistency with a smaller error bar. Through the statistical test, the samples indicated a slight increase in the RE% value. Both SF-PEG formulations had an equivalent RE%, being able to free roughly 20 µM quercetin out of the matrix after 5 minutes of ultrasound exposure.

In alignment with a previous study of using human serum albumin (HSA) and PEG in UFB systems,[26] the incorporation of PEG-400 alongside protein surfactants might enhance the release effect, as the RE% values of S10P2 and S5P2 surpassed their controls. In addition, most existing quercetin delivery systems focused on a controlled release mechanism. This is only preferable when a long time is available for drug release.

One study used a graphene oxide (GO) sheet attached with quercetin, with a loading efficiency of at most 92% and releasing efficiency of approximately less than 10% after 1–2 hours after the formulation.[71] A study using pH as a stimuli for releasing quercetin was conducted on chitosan liposomes. The results showed that the polymer scheme can enhance the

Fig. 9 Loading efficiency of samples and controls, with the report of SD error bars (* means $P < 0.05$, ns means no significant difference).
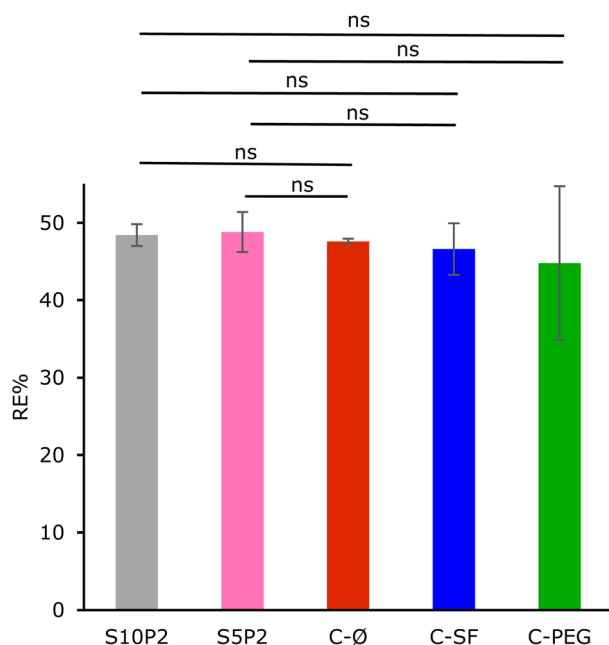
Fig. 11 Releasing efficiency of the samples and controls, with report of SD error bars (ns means no significant difference).

encapsulating efficiency but block drug release, with approximately 5% of the drug released within the first hour.[72] On the other hand, using cellulose-porous beads can produce a cumulative release of approximately 40% after 200 minutes.[73] Superparamagnetic iron nanoparticles were tested for loading and releasing quercetin under magnetic field stimulation. The RE% can achieve nearly 100%; however, the condition of the released drug was in 50% ethanol solution, and this might not reflect the true physiological condition of biological systems.[74] Another study using ultrasound to trigger the release of quercetin-coated polymer nanodroplets achieved an RE% of 3% after 5 minutes and 8% after 25 minutes.[55] Compared with these results, the UFB system might represent a promising stimuli-response mechanism for encapsulated flavonoid drug delivery. The LE% values of both samples (S10P2 and S5P2) were higher than 80%, and the RE% was nearly 50% after 5 minutes. Further pharmacokinetic and pharmacodynamic examinations can be performed to evaluate the effectiveness of the UFB system in the biological matrix. In this study, *in vitro* release analysis of the UFB systems has not been conducted because the common Franz diffusion method can cause shear stress at the pores and damage the carrier bubbles. However, with a well-protected carrier and a prolonged lifetime, these stabilized bubbles are expected to perform good drug liberation at the target site.

Conclusions

This study used silk fibroin, physiological NaCl, and conjugated PEG-400 to support an ultrasound-mediated ultrafine bubble drug transport and delivery system. Although these surfactant coatings did not substantially enhance the encapsulation

compared with the negative controls, the light scattering measurements confirmed the notable bubble stabilizing effects when incorporating both additives into the system. These stabilizing effects are crucial during the transportation of drug molecules. In addition, the adsorbed SF-PEG layer did not substantially hinder drug loading and release, as demonstrated by the 80% loading efficiency. The UFB system showed a potential triggered release mechanism with ultrasound, as it was able to release nearly 50% of the loaded content after 5 minutes of ultrasound exposure.

While these results primarily highlighted the potential of the SF-PEG conjugated bubble system, several challenges must be addressed in future research. Particularly, the interactions between surfactants, drugs, and the bubble surface are complex and not yet fully understood. More detailed surface-sensitive techniques are highly desirable to better understand the decorating adsorption layer at the air/water interface of bubbles and to deeply evaluate the performance of the delivery carrier. Future studies can also benefit from real-time imaging to track UFB dynamics, drug encapsulation, and release processes at the tissue level. Finally, to advance this silk fibroin-stabilized drug delivery system in clinical settings, *in vivo* studies are needed to gain a more comprehensive understanding of the pharmacokinetics, bioavailability, and therapeutic efficacy of UFB-based drug delivery systems.

Data availability

The data supporting this article are included in the manuscript and ESI.†

Author contributions

N. T. (investigation, methodology, writing – OD, formal analysis, and data curation), T. T. (investigation, data curation, validation, and writing – R&E), K. T. (investigation, validation, and writing – R&E), T. L. (investigation and writing – R&E), K. N. (investigation, methodology, formal analysis, data curation, and funding acquisition).

Conflicts of interest

There are no conflicts of interest to declare.

Notes and references

1 Z. Urbán-Morlán, L. E. Serrano-Mora, L. Martínez-Acevedo, G. Leyva-Gómez, N. Mendoza-Muñoz and D. Quintanar-Guerrero, in *Drug Delivery Devices and Therapeutic Systems*, 2021, pp. 601–622, DOI: 10.1016/b978-0-12-819838-4.00018-3.

2 D. Pandita, Vakar, N. Poonia, G. Chaudhary, G. K. Jain, V. Lather and R. K. Khar, in *Smart Polymeric Nano-Constructs in Drug Delivery*, 2023, pp. 65–107, DOI: 10.1016/b978-0-323-91248-8.00004-0.

3 L. Zhao, B. Wu and F. Chen, *Int. J. Pharm.*, 2023, **634**, 122704.

4 S. Kim, W.-K. Oh, Y. S. Jeong, J.-Y. Hong, B.-R. Cho, J.-S. Hahn and J. Jang, *Biomaterials*, 2011, **32**, 2342–2350.

5 M. Kakran, L. Li and R. H. Müller, *Pharm. Eng.*, 2012, **32**, 82–89.

6 S. Adepu and S. Ramakrishna, *Molecules*, 2021, **26**(19), 5905.

7 P. Vinchhi, S. U. Rawal and M. M. Patel, in *Drug Delivery Devices and Therapeutic Systems*, 2021, pp. 267–288, DOI: 10.1016/b978-0-12-819838-4.00023-7.

8 J. Jin, L. Yang, F. Chen and N. Gu, *Interdiscip. Mater.*, 2022, **1**, 471–494.

9 I. Lentacker, S. C. De Smedt and N. N. Sanders, *Soft Matter*, 2009, **5**, 2161–2170.

10 C. M. I. Quarato, D. Lacedonia, M. Salvemini, G. Tuccari, G. Mastrodonato, R. Villani, L. A. Fiore, G. Scioscia, A. Mirijello, A. Saponara and M. Sperandeo, *Diagnostics*, 2023, **13**(5), 855.

11 B. E. Polat, D. Hart, R. Langer and D. Blankschtein, *J. Controlled Release*, 2011, **152**, 330–348.

12 S.-L. Huang and D. D. McPherson, in *Cancer Theranostics*, 2014, pp. 269–283, DOI: 10.1016/b978-0-12-407722-5.00016-5.

13 M. J. K. Blomley, *Bmj*, 2001, **322**, 1222–1225.

14 H. Yusefi and B. Helfield, *Front. Phys.*, 2022, **10**, 791145.

15 I. Lentacker, S. C. De Smedt, J. Demeester, V. Van Marck, M. Bracke and N. N. Sanders, *Adv. Funct. Mater.*, 2007, **17**, 1910–1916.

16 J. P. Christiansen, B. A. French, A. L. Klibanov, S. Kaul and J. R. Lindner, *Ultrasound Med. Biol.*, 2003, **29**, 1759–1767.

17 J. L. Tlaxca, C. R. Anderson, A. L. Klibanov, B. Lowrey, J. A. Hossack, J. S. Alexander, M. B. Lawrence and J. J. Rychak, *Ultrasound Med. Biol.*, 2010, **36**, 1907–1918.

18 D. Dalecki, *Annu. Rev. Biomed. Eng.*, 2004, **6**, 229–248.

19 A. Bouakaz, M. Versluis and N. de Jong, *Ultrasound Med. Biol.*, 2005, **31**, 391–399.

20 R. Abdalkader, S. Kawakami, J. Unga, Y. Higuchi, R. Suzuki, K. Maruyama, F. Yamashita and M. Hashida, *Drug Delivery*, 2017, **24**, 320–327.

21 D. V. B. Batchelor, R. H. Abou-Saleh, P. L. Coletta, J. R. McLaughlan, S. A. Peyman and S. D. Evans, *ACS Appl. Mater. Interfaces*, 2020, **12**, 29085–29093.

22 S. Ibsen, M. Benchimol, D. Simberg, C. Schutt, J. Steiner and S. Esener, *J. Controlled Release*, 2011, **155**, 358–366.

23 C. Pellow, M. A. O'Reilly, K. Hynynen, G. Zheng and D. E. Goertz, *Nano Lett.*, 2020, **20**, 4512–4519.

24 Y. Peng, L. Zhu, L. Wang, Y. Liu, K. Fang, M. Lan, D. Shen, D. Liu, Z. Yu and Y. Guo, *Int. J. Nanomed.*, 2019, **14**, 9139–9157.

25 L. Yang, B. Huang, S. Hu, Y. An, J. Sheng, Y. Li, Y. Wang and N. Gu, *Nano Res.*, 2022, **15**, 4285–4293.

26 T. H. Le, A. H. T. Phan, K. C. M. Le, T. D. U. Phan and K. T. Nguyen, *RSC Adv.*, 2021, **11**, 34440–34448.

27 G. Guven, M. P. Hilty and C. Ince, *Blood Purif.*, 2020, **49**, 143–150.

28 R. Wu, X. Yang, X. e. Li, N. Dong, Y. Liu and P. Zhang, *J. Drug Delivery Sci. Technol.*, 2021, **65**, 102749.

29 S. Ljunggren and J. C. Eriksson, *Colloids Surf., A*, 1997, **129–130**, 151–155.

30 M. S. Plesset and S. S. Sadhal, *Appl. Sci. Res.*, 1982, **38**, 133–141.

31 J. H. Collier and P. B. Messersmith, in *Encyclopedia of Materials: Science and Technology*, 2001, pp. 602–606, DOI: 10.1016/b0-08-043152-6/00115-7.

32 G. Narsimhan and N. Xiang, *Annu. Rev. Food Sci. Technol.*, 2018, **9**, 45–63.

33 X. Qiao, R. Miller, E. Schneck and K. Sun, *Colloids Surf., A*, 2020, **591**, 124553.

34 Y. Qi, H. Wang, K. Wei, Y. Yang, R.-Y. Zheng, I. Kim and K.-Q. Zhang, *Int. J. Mol. Sci.*, 2017, **18**(3), 237.

35 T. Asakura, Y. Suzuki, Y. Nakazawa, G. P. Holland and J. L. Yarger, *Soft Matter*, 2013, **9**, 11440–11450.

36 R. M. Glaeser, *Curr. Opin. Colloid Interface Sci.*, 2018, **34**, 1–8.

37 O. Y. Milyaeva, A. V. Akentiev, A. G. Bykov, R. Miller, A. R. Rafikova, K. Y. Rotanova and B. A. Noskov, *Colloids Interfaces*, 2024, **8**(3), 35.

38 X. Qiao, R. Miller, E. Schneck and K. Sun, *Soft Matter*, 2020, **16**, 3695–3704.

39 J. J. Kwan and M. A. Borden, *Adv. Colloid Interface Sci.*, 2012, **183–184**, 82–99.

40 J. R. T. Seddon, D. Lohse, W. A. Ducker and V. S. J. Craig, *ChemPhysChem*, 2012, **13**, 2179–2187.

41 Q. Zhang, N. Wang, R. Hu, Y. Pi, J. Feng, H. Wang, Y. Zhuang, W. Xu and H. Yang, *Mater. Lett.*, 2015, **161**, 576–579.

42 A. Teimouri, M. Azadi, R. Emadi, J. Lari and A. N. Chermahini, *Polym. Degrad. Stab.*, 2015, **121**, 18–29.

43 O. Annunziata, N. Asherie, A. Lomakin, J. Pande, O. Ogun and G. B. Benedek, *Proc. Natl. Acad. Sci. U. S. A.*, 2002, **99**, 14165–14170.

44 S. Rawat, C. Raman Suri and D. K. Sahoo, *Biochem. Biophys. Res. Commun.*, 2010, **392**, 561–566.

45 K. Prasitnok and M. R. Wilson, *Phys. Chem. Chem. Phys.*, 2013, **15**, 17093–17104.

46 H. Juhling McClung, H. R. Sloan, P. Powers, A. John Merola, R. Murray, B. Kerzner and J. Dennis Pollack, *Pediatr. Res.*, 1990, **28**, 227–231.

47 Y.-S. Chen, Y.-H. Chiu, Y.-S. Li, E.-Y. Lin, D.-K. Hsieh, C.-H. Lee, M.-H. Huang, H.-M. Chuang, S.-Z. Lin, H.-J. Harn and T.-W. Chiou, *Int. J. Nanomed.*, 2019, **14**, 3601–3613.

48 M. Van Woensel, N. Wauthoz, R. Rosière, K. Amighi, V. Mathieu, F. Lefranc, S. Van Gool and S. De Vleeschouwer, *Cancers*, 2013, **5**, 1020–1048.

49 B.-q. Li, X. Dong, S.-h. Fang, J.-y. Gao, G.-q. Yang and H. Zhao, *Drug Chem. Toxicol.*, 2011, **34**, 208–212.

50 C.-F. Lin and W. L. Hayton, *Age*, 1983, **6**, 52–56.

51 S. Kumar and A. K. Pandey, *Sci. World J.*, 2013, **2013**, 1–16.

52 M. Rossi, L. F. Rickles and W. A. Halpin, *Bioorg. Chem.*, 1986, **14**, 55–69.

53 G. Cao, E. Sofic and R. L. Prior, *Free Radical Biol. Med.*, 1997, **22**, 749–760.

54 Z. Gharehnazifam, R. Dolatabadi, M. Baniassadi, H. Shahsavari, A.-M. Kajbafzadeh, K. Abrinia, K. Gharehnazifam and M. Baghani, *Int. J. Pharm.*, 2022, **621**, 121787.

55 T.-H. Tsai, L.-W. Chang, M.-L. Hou, S.-H. Hung and L.-C. Lin, *Int. J. Nanomed.*, 2015, **10**, 3031–3042.

56 A. H. T. Phan, K. C. M. Le, T. H. Le, A. V. Nguyen and K. T. Nguyen, *New J. Chem.*, 2021, **45**, 14149–14157.

57 M. A. Wheatley, F. Forsberg, N. Dube, M. Patel and B. E. Oeffinger, *Ultrasound Med. Biol.*, 2006, **32**, 83–93.

58 D. Carvalho, Â. Jesus, C. Pinho, R. F. Oliveira, F. Moreira and A. I. Oliveira, *Pharmaceuticals*, 2023, **16**(12), 1736.

59 W. Liu and R. Guo, *J. Colloid Interface Sci.*, 2006, **302**, 625–632.

60 M. Hauck, C. Noronha Martins, M. Borges Moraes, P. Aikawa, F. da Silva Paulitsch, R. D. Méa Plentz, S. Teixeira da Costa, A. M. Vargas da Silva and L. U. Signori, *Physiotherapy*, 2019, **105**, 120–125.

61 T. Prutskij, A. Deriabina, F. J. Melendez, M. E. Castro, L. Castillo Trejo, G. D. Vazquez Leon, E. Gonzalez and T. S. Perova, *Chemosensors*, 2021, **9**(11), 315.

62 J. C. Alva-Ensastegui, M. Palomar-Pardavé, M. Romero-Romo and M. T. Ramírez-Silva, *RSC Adv.*, 2018, **8**, 10980–10986.

63 M. G. Campo and G. M. Corral, *J. Phys.: Condens. Matter*, 2022, **34**(29), DOI: 10.1088/1361-648x/ac6a99.

64 W. B. Cai, H. L. Yang, J. Zhang, J. K. Yin, Y. L. Yang, L. J. Yuan, L. Zhang and Y. Y. Duan, *Sci. Rep.*, 2015, **5**, 13725.

65 Z. K. Alabri, J. Hussain, F. Mabood, N. U. Rehman, L. Ali, A. Al-Harrasi, A. Hamaed, A. L. Khan, T. S. Rizvi, F. Jabeen, A. Khan, Z. Naureen and S. Farooq, *Measurement*, 2018, **121**, 355–359.

66 S. Suzuki, R. Dawson, T. Chirila, A. Shadforth, T. Hogerheyde, G. Edwards and D. Harkin, *J. Funct. Biomater.*, 2015, **6**, 345–366.

67 P. L. Marston, D. S. Langley and D. L. Kingsbury, *Appl. Sci. Res.*, 1982, **38**, 373–383.

68 Z. Luo, B. S. Murray, A. Yusoff, M. R. A. Morgan, M. J. W. Povey and A. J. Day, *J. Agric. Food Chem.*, 2011, **59**, 2636–2645.

69 R. G. R. Pinheiro, M. Pinheiro and A. R. Neves, *Nanomaterials*, 2021, **11**(10), 2658.

70 S. S. Taher, K. K. Al-Kinani, Z. M. Hammoudi and M. m. Ghareeb, *J. Adv. Pharm. Educ. Res.*, 2022, **12**, 63–69.

71 M. Islami, A. Zarrabi, S. Tada, M. Kawamoto, T. Isoshima and Y. Ito, *Int. J. Nanomed.*, 2018, **13**, 6059–6071.

72 J. S. Seong, M. E. Yun and S. N. Park, *Carbohydr. Polym.*, 2018, **181**, 659–667.

73 T. Zhang, H. Wang, X. Pan, X. Zhang, C. Shi and X. Zhang, *J. Food Meas. Charact.*, 2024, 8233–8244.

74 L. Mandić, M. Matković, G. Baranović and S. Šegota, *Antioxidants*, 2023, **12**(3), 732.